Preprints (www.preprints.org) | NOT PEER-REVIEWED | Posted: 6 September 2022 doi:10.20944/preprints202209.0083.v1

Article

Statistical Characterization of Wireless Power Transfer via Unmodulated Emission

Sebastià Galmés [1,2,*]

[1] Departament de Ciències Matemàtiques i Informàtica, Universitat de les Illes Balears, 07122 Palma, Spain; sebastia.galmes@uib.es
[2] Institut d'Investigació Sanitària Illes Balears, 07120 Palma, Spain
* Correspondence: sebastia.galmes@uib.es

Abstract: In the past few years, the possibility to transfer power wirelessly has experienced growing interest from the research community. Since the wireless channel is subject to a large number of random phenomena, a crucial aspect is the statistical characterization of the energy that can be harvested by a given device. For this characterization to be reliable, a powerful model of the propagation channel is necessary. The recently proposed Generalized-K model has proven to be very useful, as it encompasses the effects of path-loss, shadowing and fast fading for a broad set of wireless scenarios, and it is analytically tractable. Accordingly, the purpose of this paper is to characterize, from a statistical point of view, the energy harvested by a static device from an unmodulated carrier signal generated by a dedicated source, assuming that the wireless channel obeys the Generalized-K propagation model. Specifically, using simulation-validated analytical methods, this paper provides exact closed-form expressions for the average and variance of the energy harvested over an arbitrary time period. The derived formulation can be used to determine a power transfer plan that allows multiple or even massive numbers of low-power devices to operate continuously, as expected from future network scenarios such as IoT or 5G/6G.

Keywords: RF energy harvesting; wireless power transfer; path-loss; shadowing; multi-path fading; unmodulated carrier; AWGN; mean; variance; correlation

1. Introduction

Recent developments in low-power integrated circuits and wireless technologies, the emergence of new application paradigms in the context of IoT, and a better understanding of propagation phenomena, have led the scientific community to revise Tesla's initial idea of the wireless power transfer. This idea is now seen as a promising and achievable solution to overcome the limitations of conventional power supply methods, such as batteries or wired connections to fixed power grids. Given the large number of nodes expected to be interconnected in IoT applications and other 5G/6G scenarios, the benefits of RF-EH in terms of operating cost savings and self-sustainability are undoubted. In addition, whether based solely on RF-EH or combined with other primary energy sources (solar radiation, mechanical vibration, air flow, etc.), the panacea of perpetual operation of wireless networks seems somewhat closer today.

Research in RF-EH has already produced significant results, as indicated in recent survey papers. Examples are [1], [2] and [3]. Also, relatively new books like [4] or [5] contain good compilations of the main concepts and results. However, until now less attention has been paid to the role of the propagation environment, which is crucial for the statistical characterization of the energy harvested by any device. For example, many papers assume the presence of a dedicated energy source, which performs channel estimation to adjust the transmitted power accordingly. Therefore, in these works less importance is attributed to the propagation model. However, an important application area for RF-EH is IoT, which is expected to comprise thousands or even millions of extremely simple and low-cost wireless

Preprints (www.preprints.org) | NOT PEER-REVIEWED | Posted: 6 September 2022 doi:10.20944/preprints202209.0083.v1

devices. Consequently, it is quite possible that neither these devices can participate in CSI procedures, nor can the power transmitter cope with the excessive workload involved in keeping track of each connection.

Other works adopt simplified propagation models. For example, the work presented in [6] assumes free-space path-loss and additive white Gaussian noise, which is consistent with the use of a power transmitter mounted on a UAV flying along a circular path over the wireless nodes. In [7], a two-ray model is used to account for both LOS and NLOS propagation, and then the average energy harvested is calculated. The use of the two-ray model applies to situations where there is a direct LOS component and a clear NLOS component reflected by a uniform ground plane. This model is further extended to path-loss, lognormal shadowing and Rician fading, where the latter characterizes the aggregation of many weak scattered rays rather than a single dominant one. However, such an extension is not used to obtain more general statistics on energy harvesting, but only for the estimation of experimental parameters. Reference [8] discusses a power beamforming strategy for distributed power transfer from multiple transmitters to a single receiver, based on a relatively simple path-loss model combined with Rayleigh fading and Gaussian noise. The work presented at [1] includes a brief description of wireless propagation through easy-to-handle models such as free-space, two-ray or Rayleigh.

However, among the reviewed literature, the closest contributions to the work presented in this paper are [9] and [10]. The first characterizes the average and variance of the energy collected by a node from the RF signal generated by multiple transmitters distributed according to a spatial Poisson process. The channel between each transmitter and the collector node is initially assumed to be Generalized-K, but is then approximated by a Gamma distribution and finally mixed with the rest of the channel distributions to produce a general Gaussian process according to the Central Limit Theorem. Very general propagation models are also considered in [10], such as the Generalized η-μ and κ-μ models, which are used to obtain exact closed-form expressions for the distribution, mean, variance and higher-order moments of the recharge time. However, no relationship is provided between the mathematical parameters of these models and the physical parameters of the system.

This paper fills the previous gaps by fully considering the Generalized-K propagation model for the statistical characterization of the energy collected by a single device over an arbitrary time interval. The Generalized K-model is doubly advantageous in that it is analytically tractable (in contrast to what is stated in [9]) while also covering a wide variety of scenarios with respect to all perturbations introduced by wireless channels, namely path-loss, shadowing and fast fading. Furthermore, the level of these perturbations can be easily adjusted through the model parameters, which in turn are closely related to the physical quantities that characterize the system. Specifically, closed-form expressions are obtained for the mean and variance of the energy harvested by a static device, which is assumed to be illuminated by a dedicated source emitting an unmodulated carrier. To the author's knowledge, this is the first work that adopts a very general propagation model to accurately characterize the statistics of the RF energy harvesting process. Moreover, the obtained formulation is useful for several purposes:

- To analyze the effects of system parameters on the statistics of the energy harvesting process;
- In the context of future wireless energy networks, to define guidelines for the location of primary and secondary power sources [18];
- Also with regards to wireless energy networks, to analyze the queuing behavior when multiple energy requests are directed to the same power source.

The rest of the paper is organized as follows. In Section 2, the basics of RF-EH are reviewed. In Section 3, the problem is formulated by stating the system model and assumptions, the energy harvesting equations and the Generalized-K distribution. Exact closed-form expressions for the average and variance of the energy harvested by a static device are respectively obtained in Sections 4 and 5. In Section 6, the analytical expressions are validated by simulation and then numerical results are obtained. Finally, in Section 7, the main conclusions and suggestions for further research are drawn.

2. Fundamentals of RF-EH

RF-EH has recently emerged as a disruptive technology that allows low-power portable devices and energy-constrained wireless networks to convert the electromagnetic energy present in the environment into DC current. This idea is not new, as it dates back to the early years of the last century, when Nikola Tesla designed and built an experimental station (Wardenclyffe Tower) for the wireless transfer of information and energy to remote devices. However, the project did not receive enough funds and was quickly abandoned before it became operational due to several reasons: the low efficiency of the electric-to-electromagnetic-to-electric conversion process as well as health concerns related to high power transmitters. Fortunately, in the past few years we have witnessed a resurgence of the concept, as a result of its reformulation for low power wireless devices.

WPT techniques fall into one of two major categories, namely *near-field* and *far-field*. The distinction is made because electromagnetic waves behave very differently in these two regions, and correspondingly the techniques to collect energy from them are also quite different. Near-field propagation takes place within an area of about one wavelength of the transmitting antenna, which typically corresponds to distances of at most several meters. As detailed in [3], propagation in the near-field region is essentially non-radiative, meaning that power leaves the transmitter only when there is a receiver to couple to within such region. Accordingly, power can be transferred in the near-field region by employing inductive coupling, capacitive coupling or their enhanced versions, which consist of adding resonant circuits in order to increase the power coupling coefficient and, consequently, the transmission range. However, for distances of hundreds of meters or even several kilometers, far-field is the only possible region of operation. In contrast to near-field, far-field propagation is radiative and it obeys the well-known Friis equation when no obstacles are present between transmitter and receiver. Precisely, RF-EH encompasses systems and techniques devoted to far-field WPT via electromagnetic signals like radio waves, microwaves or light waves.

The traditional receiver architecture for information decoding is not suitable for energy harvesting, not only because the goals are clearly different, but also due to the fact that the two processes work on very different power levels (much higher in the case of energy harvesting). Accordingly, one solution is to have independent segments for wireless power transfer and wireless information transfer (WIT), as depicted in Fig. 1. Such a global scenario of WIPT is also referred to as *separated receiver architecture*. As it can be noticed, power sources can be classified into two classes, *dedicated power sources* and *ambient power sources*. Dedicated power sources are specifically deployed to transfer RF energy to one or several nodes. These sources can use the license-free ISM frequency bands, though subject to restrictive upper bounds on transmission power. On the other hand, ambient power sources, that is, transmitters that are not intended for RF energy transfer, are always available at no cost, but the collected energy can be very small. So, for applications that require stable and predictable energy supply, dedicated power sources are preferable. Fig. 1 also highlights the role of a power management unit, which can implement two policies to control the incoming energy flow: *harvest-use* and *harvest-store-use*. In the harvest-use mode, the harvested energy is directly used to power the information decoder segment. Therefore, the supplied electricity has to exceed the minimum energy demand of that segment in order to guarantee its continuous operation. Otherwise, performance metrics such as delay or throughput could be penalized. The harvest-use mode is very simple to implement, but it has the disadvantage that any excess of energy is lost. By contrast, in the harvest-store-use mode, the excess energy can be stored in a rechargeable battery.

The architecture represented in Fig. 1 is also known as *out-of-band* RF energy harvesting, because the node collects energy from an RF signal different from that used to receive information. However, since the information signal also carries energy, a new

Preprints (www.preprints.org) | NOT PEER-REVIEWED | Posted: 6 September 2022 doi:10.20944/preprints202209.0083.v1

modality called SWIPT, or *in-band* energy harvesting, was devised. The new architecture is represented in Fig. 2. As it can be noticed, SWIPT allows for using a single antenna (or antenna array) to obtain both information and energy. However, a splitting architecture is required in order to distribute the received signal among the two processes. The reason is that a serial implementation would not be feasible whichever process was implemented first: either the energy harvester would destroy information, or the information decoder would consume all signal power. The splitting architecture can obey different models, namely *time-switching* and *power-splitting*. In the time-switching model, the node uses the full received signal either for information decoding or energy harvesting at a time, whereas in power-splitting the signal is divided into two streams for simultaneous information decoding and energy harvesting, not necessarily under the same power levels. References [1] and [3] provide very complete descriptions of the WIPT and SWIPT architectures. An intermediate architecture between those of Figs. 1 and 2 is one that consists of using the same RF signal to obtain information and energy, as in SWIPT, but using two different antennas (or two sets of antenna arrays) at the receiving node, as in WIPT, in order to avoid the splitting process. In [3], this architecture is referred to as *antenna-switching*, thus essentially a new form of splitting architecture.

Finally, another architecture is *frequency-splitting*, whose diagram is shown in Fig. 3. In this architecture, the input signal transports both information and power by using separated frequencies. In fact, this signal consists of the information-bearing modulated component plus an unmodulated sine wave that essentially results from shifting the carrier frequency used in the modulation process, from a value f_c to a different value f_p. The figure also highlights the fact that though the transmitter sends a pure sinusoidal to transfer power, the received signal exhibits some spread due to variations in channel coefficient. So, there must be a sufficiently high guard band between f_c and f_p.

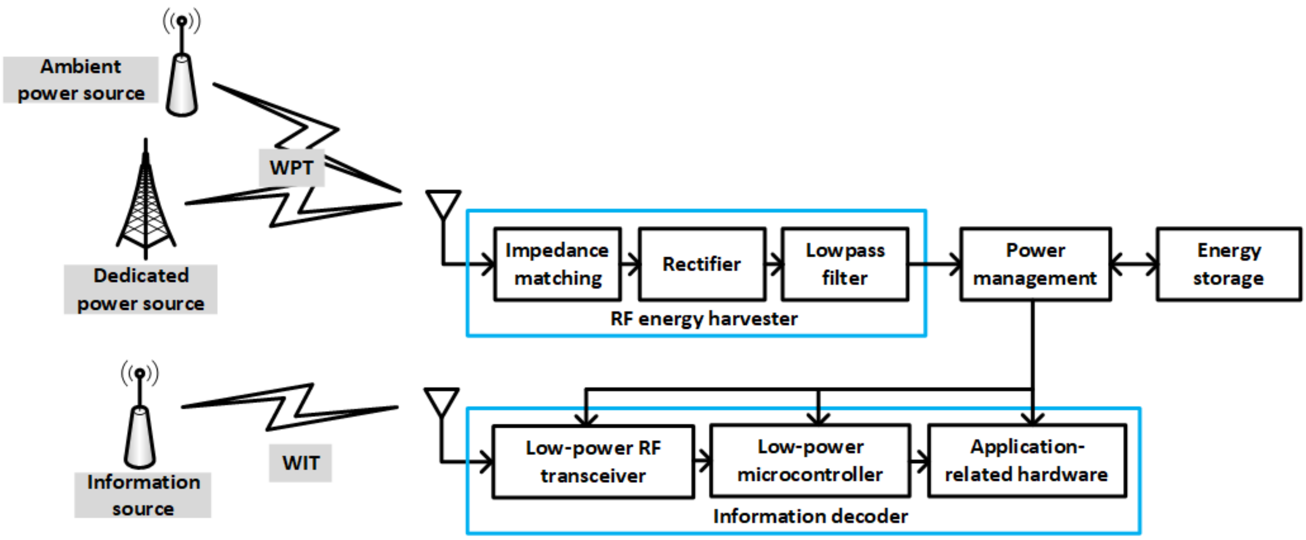

Figure 1. WIPT scenario, with separated WIT and WPT segments. The WIT segment contains conventional hardware to receive (and also transmit) information, whereas the WPT segment is essentially a voltage rectifier followed by a low-pass filter devoted to extracting the DC component of the received signal.

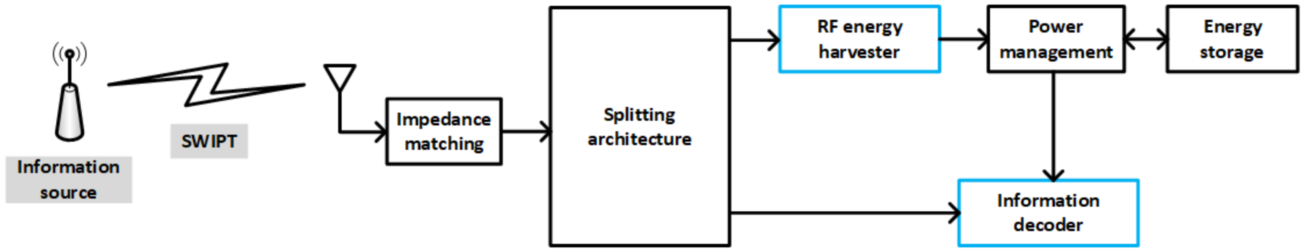

Figure 2. SWIPT scenario. Power is obtained from the same information signal, by using a splitting architecture that generates an input for every independent process.

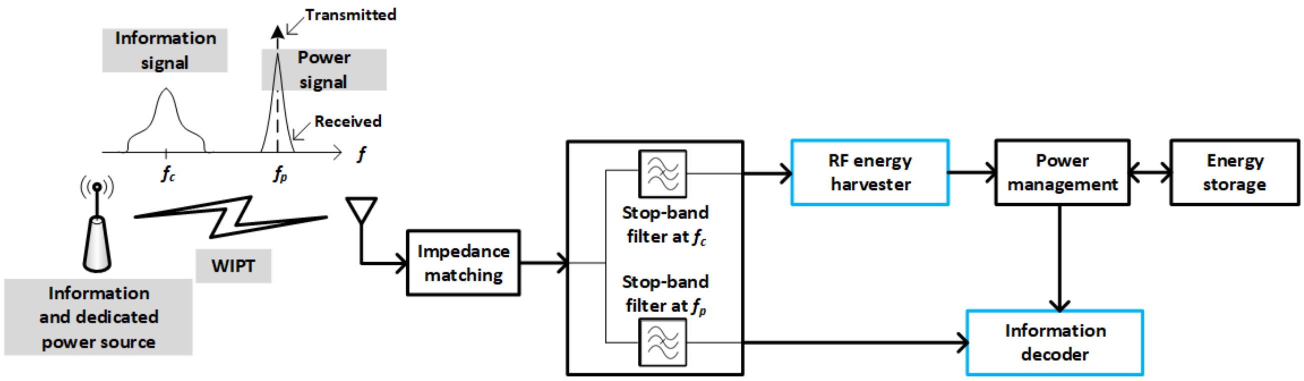

Figure 3. Frequency-splitting architecture. This architecture is really a variant of WIPT, because information and power are transferred via signals differentiated in the frequency domain. However, just a single antenna is required at each side of the link, as in SWIPT.

3. Problem Formulation

In this section, the system model and assumptions, the fundamental energy harvesting equation and the Generalized-K distribution are formulated.

3.1. System Model and Assumptions

As stated in [1], the SWIPT architectures always impose a trade-off between information rate and amount of RF energy harvested. To bypass this trade-off, specially in situations where stable and predictable energy supply is required, WPT from a dedicated source is preferable. Accordingly, this paper focuses on scenarios like those shown in Fig. 1 or Fig. 3. More specifically, the system under analysis is shown in Fig. 4, where a dedicated power source generates an unmodulated carrier at frequency f_p in the RF, microwave or visible light bands. Both the power source and the receivers are located at fixed positions and equipped with directional antennas of gains G_t and G_r respectively. In particular, the power source uses a phased array that allows for tuning the main beam in the direction of current receiver, whereas receiver antennas are always aligned with the power source. An AWGN channel is assumed, with spectral noise density N_0 and a channel coefficient $h(t)$ that obeys the above-mentioned Generalized-K distribution. Also, the energy harvesting device is assumed to operate linearly, in spite of the presence of non-linear components like diodes. For the sake of generality, the analysis will start from an arbitrary waveform $x(t)$ for the power-bearing signal, and only in the end it will be particularized to the special case of an unmodulated carrier. The corresponding power transfer bandwidth is B, meaning that the impedance matching circuit (or the combined effect of this circuit and the stop-band filter at f_c if the scenario of Fig. 3 is considered) has an equivalent bandwidth B centered at frequency f_p.

Preprints (www.preprints.org) | NOT PEER-REVIEWED | Posted: 6 September 2022 doi:10.20944/preprints202209.0083.v1

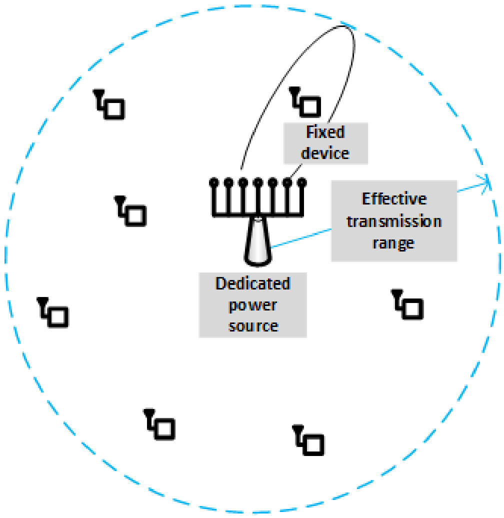

Figure 4. System model.

3.2. Energy Harvesting Equation

Using complex notation, the power-bearing signal $x(t)$ can be expressed in terms of its equivalent low-pass signal or complex envelope $\tilde{x}(t)$ as follows:

$$x(t) = \Re\left\{\tilde{x}(t) \cdot e^{j2\pi f_p t}\right\} \tag{1}$$

Here, $\Re$ stands for the real part. As pointed out in [12], the received signal can be generally formulated in this way:

$$r(t) = \Re\left\{\sum_{k=0}^{K(t)} \alpha_k(t) \cdot \tilde{x}(t - \tau_k(t)) \cdot e^{j\left(2\pi f_p (t - \tau_k(t)) + \varphi_k\right)}\right\} + n(t) \tag{2}$$

In this expression, $n(t)$ is the AWGN component, $K(t)$ is the total number of resolvable multi-path components and $\alpha_k(t)$, $\tau_k(t)$ and ϕ_k are, respectively, the time-dependent amplitude and delay parameters and a constant phase offset associated with the k:th resolvable multi-path component. If the delay spread of the channel, T_m, verifies $T_m \ll \frac{1}{B}$, then $\tilde{x}(t - \tau_k(t)) \cong \tilde{x}(t)$. This is the so called narrow-band fading condition. Note that for $x(t)$ consisting of an unmodulated carrier, this condition holds for any T_m. So, under narrow-band fading, we have:

$$r(t) = \Re\left\{\left(\sum_{k=0}^{K(t)} \alpha_k(t) \cdot e^{-j\left(2\pi f_p \tau_k(t) - \varphi_k\right)}\right) \cdot \tilde{x}(t) \cdot e^{j2\pi f_p t}\right\} + n(t) \tag{3}$$

The summation term between parentheses is independent of the complex envelope $\tilde{x}(t)$ and hence it simply introduces a multiplicative effect on the signal. It's the so called channel coefficient, typically denoted by $h(t)$. Accordingly, equation (3) can be rewritten in the following way:

$$r(t) = \Re\left\{\tilde{x}(t) \cdot h(t) \cdot e^{j2\pi f_p t}\right\} + n(t) \tag{4}$$

The noise component can also be reformulated in terms of its complex envelope $\tilde{n}(t)$ as $n(t) = \Re\{\tilde{n}(t) \cdot e^{j2\pi f_p t}\}$, and therefore the channel output signal can be expressed as follows:

$$r(t) = \Re\left\{(\tilde{x}(t) \cdot h(t) + \tilde{n}(t)) \cdot e^{j2\pi f_p t}\right\} \tag{5}$$

The term multiplying the exponential is nothing else but the complex envelope of the received signal $r(t)$, namely $\tilde{r}(t)$:

Preprints (www.preprints.org) | NOT PEER-REVIEWED | Posted: 6 September 2022 doi:10.20944/preprints202209.0083.v1

$$\tilde{r}(t) = \tilde{x}(t) \cdot h(t) + \tilde{n}(t) \tag{6}$$

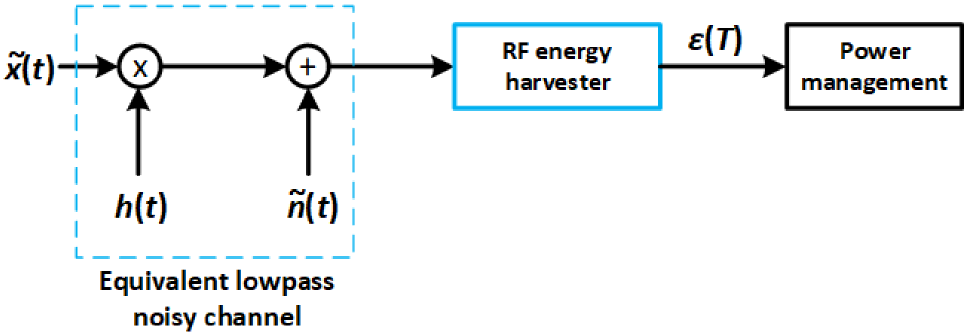

Figure 5. Equivalent low-pass model of the channel.

Fig. 5 shows the equivalent low-pass representation of the channel effect, as well as the subsequent energy harvesting and power management units. The energy harvesting unit is capable of producing a certain amount of energy at the end of an exposition time period T. This energy, denoted as $\mathcal{E}(T)$, can be mathematically formulated as follows:

$$\mathcal{E}(T) = \eta \int_T r^2(t) \cdot dt \tag{7}$$

Here, the integral represents the RF energy captured by the receiving antenna along the period T, whereas η denotes the RF-to-DC conversion efficiency. Equation (7) constitutes the starting point of the analysis performed in this paper.

3.3. The Generalized-K Distribution

The Generalized-K distribution is a powerful description of the perturbation effects experienced by signals in wireless propagation environments. It was proposed at the beginning of the 2000 decade as a compound probability density function (PDF) encompassing all sources of wireless signal degradation, namely path-loss, shadowing and fast fading. In addition, it enjoys the property of analytical tractability, which helps to obtain closed-form expressions for the performance measures of interest. An example is the statistical characterization of the energy harvested performed in this paper. The availability of closed-form expressions for magnitudes such as the mean and variance of the energy harvested is very useful for network planning, specially in scenarios like IoT, where the energy provider cannot rely on CSI to adjust its transmission power because of the expected massive number of participating devices.

The Generalized-K model combines the Nakagami-m distribution for fast fading and the Gamma distribution for path-loss and shadowing (Nakagami-Gamma). In addition, it can be particularized to numerous well-known models, such as Rayleigh-Lognormal (Suzuki model), Nakagami-Lognormal, Rayleigh-Gamma (K model) and, in an approximate way, Rician-Gamma and Rician-Lognormal.

Let $z = z(t) = \|h(t)\|$ be the module of the channel coefficient. Assuming that the channel is stationary, z can be treated as a single random variable whose statistical characterization is independent of time. If the Nakagami distribution is used to model small-scale multi-path fading whereas the Gamma distribution is used to model path-loss and shadowing, the resulting composite fading process obeys the Generalized-K model. Accordingly, the probability density function (PDF) of z can be expressed as follows:

$$f_Z(z) = \frac{4\sqrt{\frac{m}{b}}}{\Gamma(a)\Gamma(m)} \left(\sqrt{\frac{m}{b}}z\right)^{a+m-1} K_{a-m}\left(2\sqrt{\frac{m}{b}}z\right) \tag{8}$$

Preprints (www.preprints.org) | NOT PEER-REVIEWED | Posted: 6 September 2022 doi:10.20944/preprints202209.0083.v1

In this expression, a and b are respectively the shape and scale parameters of the Gamma distribution ($a > 0$, $b > 0$), whereas $m > 0$ is the so-called Nakagami parameter. K_{a-m} stands for the modified Bessel function of order $(a - m)$. In turn, a and b can be formulated in terms of physical parameters:

$$a = \frac{1}{e^{\frac{\sigma^2_{\Psi dB}}{\zeta^2}} - 1} \tag{9}$$

$$b = e^{\frac{\mu_{\Psi dB}}{\zeta} + \frac{\sigma^2_{\Psi dB}}{2\zeta^2}} \left(e^{\frac{\sigma^2_{\Psi dB}}{\zeta^2}} - 1 \right) \tag{10}$$

In these expressions, $\zeta = \frac{10}{\ln 10}$, and $\mu_{\Psi dB}$ and $\sigma_{\Psi dB}$ are, respectively, the average and standard deviation of $\Psi dB = 10 \log_{10} \Psi = 10 \log_{10} \frac{P_r}{P_t}$, that is, the ratio of power received to power transmitted expressed in dB. The expected value $\mu_{\Psi dB}$ is given by the following expression:

$$\mu_{\Psi dB} = 10 \log_{10} \alpha - 10\beta \log_{10} \frac{d}{d_0} \tag{11}$$

Here, d is the distance between the transmitter and the receiver (transmission distance), d_0 is the reference distance, β is the path-loss exponent and α is a constant that depends on multiple parameters (antenna gains, reference distance, path-loss exponent, average blockage and carrier frequency). There is no mathematical expression for $\sigma_{\Psi dB}$ (shadowing spread), but it's value has been experimentally set up within the range $[4, 13]$ dB [12]. The generic path-loss model given in (11) can be replaced by more specific models (free-space, two-ray, Okumura, Hata, COST 231, etc.) when further details about the scenario are provided [12].

Equations (8) to (11) define a versatile propagation model that is entirely formulated in terms of physical (and measurable) parameters. To summarize, the inputs to this model are the constant α, the path-loss exponent, both the transmission and reference distances, the delay spread and the Nakagami parameter. This parameter can take on any value above 0, thus providing high flexibility to capture quite different small-scale multi-path fading conditions:

- If $m > 1$, the channel is Rician, meaning that there is a dominant line-of-sight (LOS) propagation component over the scattered non-LOS component. This is the so-called *non-isotropic propagation environment*. In this case, the degree of fading is low, becoming less severe with increasing m. In particular, for $m \to \infty$ there is no fading.
- If $m \leq 1$, there is no dominant LOS component in the received signal and the degree of fading is high, increasing as m decreases. Such scenario is referred to as *isotropic propagation environment*. Particular cases are $m = 1$ (Rayleigh channel), $m = 0.5$ (one-sided Gaussian channel) and $m \ll 1$ (very severe fading channel).

4. Average Energy Harvested

The first step in the characterization of the amount of energy harvested as a random variable is to obtain its average. Recalling equation (7), the expected energy harvested can be formulated in this way:

$$E\{\mathcal{E}(T)\} = E\left\{\eta \int_T r^2(t) \cdot dt\right\} = \eta \int_T E\left\{r^2(t)\right\} \cdot dt = \frac{\eta}{2} \int_T E\left\{\|\tilde{r}(t)\|^2\right\} \cdot dt \tag{12}$$

On the other hand, from equation (7), we have:

$$\tilde{r}(t) = \left(\tilde{x}_I(t) + j \cdot \tilde{x}_Q(t)\right) \cdot \left(h_{re}(t) + j \cdot h_{im}(t)\right) + \tilde{n}_I(t) + j \cdot \tilde{n}_Q(t) \tag{13}$$

In this expression, both $\tilde{x}(t)$ and $\tilde{n}(t)$ have been decomposed into their in-phase and quadrature components, respectively $(\tilde{x}_I(t), \tilde{x}_Q(t))$ and $(\tilde{n}_I(t), \tilde{n}_Q(t))$, and the channel

Preprints (www.preprints.org) | NOT PEER-REVIEWED | Posted: 6 September 2022 doi:10.20944/preprints202209.0083.v1

coefficient into its real and imaginary parts, namely $(h_{re}(t), h_{im}(t))$. Further manipulation allows to separate the real and imaginary components of $\tilde{r}(t)$ as follows:

$$\tilde{r}(t) = \tilde{x}_I(t) \cdot h_{re}(t) - \tilde{x}_Q(t) \cdot h_{im}(t) + \tilde{n}_I(t) + j \cdot \left(\tilde{x}_I(t) \cdot h_{im}(t) + \tilde{x}_Q(t) \cdot h_{re}(t) + \tilde{n}_Q(t)\right) \tag{14}$$

Then, the squared module of $\tilde{r}(t)$ is nothing else but the sum of the squared real and imaginary parts:

$$\|\tilde{r}(t)\|^2 = \left(\tilde{x}_I(t) \cdot h_{re}(t) - \tilde{x}_Q(t) \cdot h_{im}(t) + \tilde{n}_I(t)\right)^2 + \left(\tilde{x}_I(t) \cdot h_{im}(t) + \tilde{x}_Q(t) \cdot h_{re}(t) + \tilde{n}_Q(t)\right)^2 \tag{15}$$

Proceeding through standard calculations, we can end up with the following exact result for $\|\tilde{r}(t)\|^2$:

$$\begin{aligned}\|\tilde{r}(t)\|^2 = \|\tilde{x}(t)\|^2 \cdot \|h(t)\|^2 + \tilde{n}_I^2(t) + \tilde{n}_Q^2(t) + 2\left(\tilde{x}_I(t) \cdot h_{re}(t) - \tilde{x}_Q(t) \cdot h_{im}(t)\right) \cdot \tilde{n}_I(t) \\ + 2\left(\tilde{x}_I(t) \cdot h_{im}(t) + \tilde{x}_Q(t) \cdot h_{re}(t)\right) \cdot \tilde{n}_Q(t)\end{aligned} \tag{16}$$

Next, we can obtain the expectation of $\|\tilde{r}(t)\|^2$. The analysis can be simplified by recalling some valuable properties of AWGN ([14]): (*i*) $E\{\tilde{n}_I^2(t)\} = E\left\{\tilde{n}_Q^2(t)\right\} = E\{n^2(t)\} = N_R = \eta_0 \cdot B$, where N_R stands for the received noise power, η_0 for the spectral density power and B for the power transfer bandwidth, (*ii*) $E\{\tilde{n}_I(t)\} = E\{\tilde{n}_Q(t)\} = 0$, and (*iii*) $\tilde{n}_I(t)$ and $\tilde{n}_Q(t)$ are mutually independent Gaussian random variables. In addition, since noise is independent of both, input signal and channel coefficient, and $E\{\tilde{n}_I(t)\} = 0$, we also have $E\{\left(\tilde{x}_I(t) \cdot h_{re}(t) - \tilde{x}_Q(t) \cdot h_{im}(t)\right) \cdot \tilde{n}_I(t)\} = E\{\left(\tilde{x}_I(t) \cdot h_{re}(t) - \tilde{x}_Q(t) \cdot h_{im}(t)\right)\} \cdot E\{\tilde{n}_I(t)\} = 0$. Similarly, $E\{\left(\tilde{x}_I(t) \cdot h_{im}(t) + \tilde{x}_Q(t) \cdot h_{re}(t)\right) \cdot \tilde{n}_Q(t)\} = 0$. Because the input signal and the channel coefficient are also mutually independent random variables, the squared module of the complex envelope can be expressed in this way:

$$E\left\{\|\tilde{r}(t)\|^2\right\} = E\left\{\|\tilde{x}(t)\|^2\right\}E\left\{\|h(t)\|^2\right\} + 2E\left\{n^2(t)\right\} \tag{17}$$

Accordingly, the average energy harvested formulated in (12) obeys the following expression:

$$E\{\mathcal{E}(T)\} = \eta \int_T \left(\frac{E\{\|\tilde{x}(t)\|^2\}}{2} E\left\{\|h(t)\|^2\right\} + E\left\{n^2(t)\right\}\right) \cdot dt \tag{18}$$

The equivalent low-pass input signal $\tilde{x}(t)$ is defined by the modulation. So, in principle, $\tilde{x}(t) = A(t)e^{j\theta(t)}$, where $A(t)$ and $\theta(t)$ denote, respectively, the time-varying amplitude and phase of the modulating signal. So, in general, $\|\tilde{x}(t)\|^2$ is not a stationary process, which means that its expectation is not time-independent and cannot be taken out of the integral in the above equation. So, under these conditions, at most we can write:

$$E\{\mathcal{E}(T)\} = \eta \int_T \left(\frac{E\{A^2(t)\}}{2} E\left\{\|h(t)\|^2\right\} + N_R\right) \cdot dt \tag{19}$$

In [13], exact closed-form expressions for the moments of the Generalized-K distribution are provided, among which the second moment is given by $E\{\|h(t)\|^2\} = a \cdot b$, where a and b obey, respectively, expressions (9) and (10). This second moment is nothing else but the contribution of the channel to the expected value of the squared envelope of the received signal. In agreement with [17], this contribution will be renamed from now on as Ω_p. So, in summary, Ω_p represents the global channel effect on the transmitted power, as it includes path-loss, shadowing and multi-path fading. Accordingly, the average energy harvested can be rewritten as follows:

$$E\{\mathcal{E}(T)\} = \eta \int_T \left(\frac{E\{A^2(t)\}}{2} \cdot \Omega_p + N_R\right) \cdot dt \tag{20}$$

Preprints (www.preprints.org) | NOT PEER-REVIEWED | Posted: 6 September 2022 doi:10.20944/preprints202209.0083.v1

Finally, if the input signal corresponds to an unmodulated carrier, then $A(t) = A$ and the previous equation can be reformulated in a simpler way:

$$E\{\mathcal{E}(T)\} = \eta \cdot T\left(\frac{A^2}{2} \cdot \Omega_p + N_R\right) \quad (21)$$

The term $\frac{A^2}{2}$ is nothing else but the transmitted power (normalized to a 1Ω-load). If we denote this power as P_t, the expected energy harvested is as follows:

$$E\{\mathcal{E}(T)\} = \eta \cdot T(P_t \cdot \Omega_p + N_R) \quad (22)$$

Note that the average energy harvested depends on the shape and scale parameters of the Gamma distribution (via Ω_p), but not on the Nakagami parameter that characterizes multipath fading. Note also that it has two components, the main one due to the power-bearing signal, and the thermal noise.

5. Variance of Energy Harvested

To obtain the variance of the energy harvested, first we can analyze the second moment about zero:

$$\begin{aligned} E\left\{\mathcal{E}^2(T)\right\} &= \eta^2 E\left\{\left(\int_T r^2(t)dt\right)^2\right\} = \eta^2 E\left\{\left(\int_T r^2(s)ds\right)\left(\int_T r^2(t)dt\right)\right\} \\ &= \eta^2 E\left\{\int_T\int_T r^2(s)r^2(t)ds\cdot dt\right\} = \eta^2\int_T\int_T E\left\{r^2(s)r^2(t)\right\}ds\cdot dt \\ &= \frac{\eta^2}{4}\int_T\int_T E\left\{\|\tilde{r}(s)\|^2\|\tilde{r}(t)\|^2\right\}ds\cdot dt \end{aligned} \quad (23)$$

The next step is to evaluate the expectation inside the integral, which is nothing else but a correlation. However, the analytical procedure that yields an exact closed-form expression for this correlation is very complex, and thus the details have been relegated to the Appendix. Setting $s = t + \tau$, the result is - equation (A.31):

$$\begin{aligned} E\left\{\|\tilde{r}(t+\tau)\|^2\|\tilde{r}(t)\|^2\right\} &= \phi_{\|\tilde{r}\|^2}(t,\tau) = \phi_{\|\tilde{x}\|^2}(t,\tau)\phi_{\|h\|^2}(\tau) + 4N_R \cdot E\left\{\|\tilde{x}(t)\|^2\right\}E\left\{\|h(t)\|^2\right\} \\ &+ 16\phi_{\tilde{n}}(\tau)\cdot\Re\{\phi_{\tilde{x}}(t,\tau)\phi_h(\tau)\} + 4N_R^2 + 4\phi_{\tilde{n}}^2(\tau) \end{aligned} \quad (24)$$

Next, the terms that appear in this equation are analyzed individually.

If we assume that the input signal is an unmodulated carrier, that is, $\tilde{x}(t) = Ae^{j\theta}$, we have:

$$E\left\{\|\tilde{x}(t)\|^2\right\} = A^2 = 2P_t \quad (25)$$

$$\phi_{\|\tilde{x}\|^2}(t,\tau) = E\left\{\|\tilde{x}(t+\tau)\|^2\|\tilde{x}(t)\|^2\right\} = A^4 = 4P_t^2 \quad (26)$$

$$\phi_{\tilde{x}}(t,\tau) = \frac{1}{2}E\{\tilde{x}(t+\tau)\tilde{x}^*(t)\} = \frac{1}{2}E\left\{Ae^{j\theta}\cdot Ae^{-j\theta}\right\} = \frac{A^2}{2} = P_t \quad (27)$$

Note that, for the case of an unmodulated carrier, the input signal does not only become a stationary process, but its associated correlations are constant. Also, despite it has been assumed that θ is a constant phase offset, the analysis that follows would also be valid, with some minor modifications, for a phase-modulated signal, that is, $\theta = \theta(t)$.

Another auto-correlation involved in (24) is $\phi_{\tilde{n}}(\tau)$. For the case of AWGN, the following expression is provided in [14]:

$$\phi_{\tilde{n}}(\tau) = \eta_0\frac{\sin(\pi B\tau)}{\pi\tau} = \eta_0 B\frac{\sin(\pi B\tau)}{\pi B\tau} = N_R(\pi B\tau) \quad (28)$$

Preprints (www.preprints.org) | NOT PEER-REVIEWED | Posted: 6 September 2022 doi:10.20944/preprints202209.0083.v1

The remaining terms are $\phi_h(\tau)$ and $\phi_{||h||^2}(\tau)$, which are channel auto-correlations. They capture the variations, in statistical sense, perceived by the user as it moves at certain speed v over the combined path-loss, shadowing and multi-path fading scenario under consideration (in the present case, the scenario that leads to the Generalized-K distribution). These temporal correlations can always be transformed into spatial correlations, since the dependence on τ is, in fact, on the product $v \cdot \tau$. However, because the focus of this paper is on static users, that is, $v = 0$, which has the same effect as $\tau = 0$, we are really interested in $\phi_h(0)$ and $\phi_{||h||^2}(0)$. Regarding the first one, we can write:

$$\phi_h(0) = \frac{1}{2}E\{h(t) \cdot h^*(t)\} = \frac{1}{2}E\left\{||h(t)||^2\right\} = \frac{\Omega_p}{2} \tag{29}$$

To analyze the second term, it is useful to introduce the auto-covariance $\mu_{||h||^2}(\tau)$, which is related to the auto-correlation as follows:

$$\mu_{||h||^2}(\tau) = \phi_{||h||^2}(\tau) - E\left\{||h(t+\tau)||^2\right\} \cdot E\left\{||h(t)||^2\right\} \tag{30}$$

Accordingly:

$$\phi_{||h||^2}(0) = \mu_{||h||^2}(0) + E^2\left\{||h(t)||^2\right\} = \mu_{||h||^2}(0) + \Omega_p^2 \tag{31}$$

Since the auto-covariance at the origin is nothing else but the variance, we have:

$$\phi_{||h||^2}(0) = Var\left\{||h(t)||^2\right\} + \Omega_p^2 \tag{32}$$

Moreover, $Var\{||h(t)||^2\}$ can be expressed in terms of the second and fourth moments of the distribution of $||h(t)||$:

$$Var\left\{||h(t)||^2\right\} = E\left\{||h(t)||^4\right\} - E^2\left\{||h(t)||^2\right\} \tag{33}$$

Note that the second term in the right-hand side of this equation is Ω_p^2. In [13], a generic closed-form expression is provided for the moments of the Generalized-K distribution. This expression is exact and can be particularized for the fourth moment as follows:

$$E\left\{||h(t)||^4\right\} = \frac{\Gamma(a+2)\Gamma(m+2)}{\Gamma(a)\Gamma(m)}\left(\frac{b}{m}\right)^2 \tag{34}$$

Recall that a and b are, respectively, the scale and shape parameters of the Gamma distribution that describes path-loss and shadowing, and m is the Nakagami parameter that characterizes multi-path fading. Next, considering equations (33) and (34), equation (32) can be rewritten in terms of the parameters of the Generalized-K distribution:

$$\phi_{||h||^2}(0) = \frac{\Gamma(a+2)\Gamma(m+2)}{\Gamma(a)\Gamma(m)}\left(\frac{b}{m}\right)^2 \tag{35}$$

Now, introducing (25), (26), (27), (28), (29) and (35) into equation (24), and rearranging terms, we can obtain the definite result for $E\{||\tilde{r}(t+\tau)||^2||\tilde{r}(t)||^2\}$:

$$\begin{aligned} E\left\{||\tilde{r}(t+\tau)||^2||\tilde{r}(t)||^2\right\} &= 4P_t^2\frac{\Gamma(a+2)\Gamma(m+2)}{\Gamma(a)\Gamma(m)}\left(\frac{b}{m}\right)^2 \\ &+ 8N_R P_t \Omega_p(1+(\pi B\tau)) \\ &+ 4N_R^2(1+^2(\pi B\tau)) \end{aligned} \tag{36}$$

As it can be noticed, this expression depends exclusively on system parameters. In particular, $P_t\Omega_p$ is the average received power, since it is the product of the average transmitted power and the channel effect represented by Ω_p. Finally, the variance of the energy har-

Preprints (www.preprints.org) | NOT PEER-REVIEWED | Posted: 6 September 2022 doi:10.20944/preprints202209.0083.v1

vested can be obtained by integrating expression (36) according to (23), and then subtracting the square of the expected energy harvested given by (22). An exact closed-form expression is obtained:

$$\begin{aligned} Var\{\mathcal{E}(T)\} &= (\eta P_t T)^2 \left(\frac{\Gamma(a+2)\Gamma(m+2)}{\Gamma(a)\Gamma(m)} \left(\frac{b}{m}\right)^2 - \Omega_p^2 \right) \\ &+ \frac{4\eta^2 N_R P_t \Omega_p}{\pi^2 B^2} (-1 + \cos(\pi BT) + \pi BT \cdot Si(\pi BT)) \\ &+ \frac{\eta^2 N_R^2}{\pi^2 B^2} \Big(-1 - \gamma + \cos(2\pi BT) + Ci(2\pi BT) \\ &- \ln(2\pi BT) + 2\pi BT \cdot Si(2\pi BT) \Big) \end{aligned} \tag{37}$$

Here, γ is the Euler's constant ($\gamma \simeq 0.577216$) and $Si()$ and $Ci()$ stand respectively for the sine integral and cosine integral functions, which are defined as follows:

$$Si(x) = \int_0^x \frac{\sin(u)}{u} du \tag{38}$$

$$Ci(x) = -\int_x^\infty \frac{\cos(u)}{u} du \tag{39}$$

As it can be noticed from equation (37), the variance of the energy harvested has three components: one that depends exclusively on the power-bearing signal, a cross-term that depends on both the power-bearing signal and the thermal noise, and finally a third component that only depends on noise.

The squared coefficient of variation of the energy harvested, namely $SCV\{\mathcal{E}(T)\}$, is given by:

$$\begin{aligned} SCV\{\mathcal{E}(T)\} &= P_t^2 \frac{\left(\frac{\Gamma(a+2)\Gamma(m+2)}{\Gamma(a)\Gamma(m)} \left(\frac{b}{m}\right)^2 - \Omega_p^2 \right)}{(P_t\Omega_p + N_R)^2} \\ &+ \frac{4 N_R P_t \Omega_p (-1 + \cos(\pi BT) + \pi BT \cdot Si(\pi BT))}{\pi^2 B^2 T^2 (P_t \Omega_p + N_R)^2} \\ &+ \frac{N_R^2}{\pi^2 B^2 T^2 (P_t \Omega_p + N_R)^2} \Big(-1 - \gamma + \cos(2\pi BT) \\ &+ Ci(2\pi BT) - \ln(2\pi BT) + 2\pi BT \cdot Si(2\pi BT) \Big) \end{aligned} \tag{40}$$

If the signal-to-noise ratio is very high, we can approximate the squared coefficient of variation of the energy harvested ($SCV\{\mathcal{E}(T)\}$) by the next limit:

$$\lim_{N_R \to 0} SCV\{\mathcal{E}(T)\} = \frac{\Gamma(a+2)\Gamma(m+2)}{\Gamma(a)\Gamma(m)\Omega_p^2} \left(\frac{b}{m}\right)^2 - 1 \tag{41}$$

Recall that $\Omega_p = a \cdot b$. Equation (41) is nothing else but the squared coefficient of variation of $\|h(t)\|^2$.

6. Validation and Performance Assessment

In this section, the analysis performed in this paper is validated via simulation, and then the evolution of $E\{\mathcal{E}(T)\}$ and $SCV\{\mathcal{E}(T)\}$ in terms of multiple input variables is studied. With no loss of generality, an exposition time of 1 minute is assumed. To highlight the possibilities of the RF energy harvesting technology, a long-range scenario is considered, which is based on a real case: the KING-TV tower located at Seattle (Washington, US). This telecommunications tower transmits several analog and digital TV channels in the VHF and UHF bands respectively. Particularly, it uses a source power of 960 kW to broadcast a

Preprints (www.preprints.org) | NOT PEER-REVIEWED | Posted: 6 September 2022 doi:10.20944/preprints202209.0083.v1

6-MHz digital TV signal at the frequency of 0.677 GHz. The evaluation that follows assumes that all transmit power is concentrated on this frequency ($f_p = 0.677$ GHz), though the receiver bandwidth is kept to 6 MHz ($B = 6$ MHz). Other fixed parameters are the reference distance ($d_0 = 1$ m), the energy conversion efficiency ($\eta = 0.5$), the ambient temperature (290 K) and the receiver noise figure (9 dB).

For the simulation and performance assessment, four input variables were taken into consideration: the transmission distance, the path-loss exponent, the shadowing spread and the Nakagami parameter. Accordingly, Table 1 shows the analytical and simulation results for both the expected and squared coefficient of variation of the energy harvested. For each set of values, at least 30000 runs were executed in order to achieve relative errors within 10% at a 90% confidence level. As it can be noticed from the table, there is high agreement between analytical and simulation results.

Table 1. Comparison between analytical and simulation results for different parameter sets.

d**(m)**, β, $\sigma_{\Psi dB}$, m	$E\{\mathcal{E}(T)\}$ **analytical** $SCV\{\mathcal{E}(T)\}$ **analytical**	$E\{\mathcal{E}(T)\}$ **simulation** $SCV\{\mathcal{E}(T)\}$ **simulation**
10000, 4.0, 4.5, 1.0	0.000618319 4.76260	0.000615756 4.63304
10000, 3.0, 8.5, 2.0	24.3135 68.1367	25.1643 68.2532
20000, 2.0, 6.5, 4.0	27440.9 10.7423	26991.4 10.0688
20000, 3.0, 8.5, 5.0	3.03919 54.3092	2.9721 54.1187
30000, 3.5, 6.5, 7.0	0.00235284 9.6885	0.00233108 9.19882
30000, 2.5, 4.5, 9.0	39.2981 2.2511	39.7297 2.24226
40000, 2.0, 6.5, 10.0	6860.24 9.3332	6774.42 8.927
40000, 4.0, 8.5, 6.0	0.0000152195 20.5507	0.0000151148 19.1669
50000, 2.5, 4.5, 3.0	10.9585 2.90132	11.0875 2.7808
50000, 3.5, 10.5, 8.0	0.00238773 385.967	0.00235364 361.542
60000, 3.0, 8.0, 5.0	0.0904563 34.7094	0.0897801 33.9685
60000, 2.0, 4.0, 10.0	1520.35 1.56925	1529.88 1.551
70000, 2.5, 6.0, 1.0	7.17395 12.4884	7.23829 12.2202
70000, 3.5, 5.0, 5.0	0.0000822848 3.04467	0.0000825077 3.03913
80000, 4.0, 10.0, 3.0	$6.96074 \cdot 10^{-6}$ 8.44362	$6.95204 \cdot 10^{-6}$ 8.39472
80000, 3.0, 7.0, 7.0	0.0256447 14.3489	0.0253276 13.7613
90000, 2.5, 10.5, 6.0	27.3988 402.224	27.1551 407.723
90000, 3.5, 8.0, 1.0	0.0000950559 51.6893	0.0000937424 50.6754
100000, 2.0, 7.5, 4.0	1590.89 23.6669	1523.16 23.0866
100000, 3.0, 4.5, 2.0	0.00613169 3.38267	0.00616622 3.43746

To assess the performance of the energy harvesting process, several input-output relations were explored, the results of which are reflected in subsequent figures. For instance, Figure 6 plots the evolution of the average energy harvested in terms of distance for different values of the path-loss exponent. As expected, the average energy harvested increases as the distance and the path-loss exponent decrease. A similar plot is shown in Figure 7, but parameterized by the shadowing spread instead of the path-loss exponent. The figure reveals that the average energy harvested increases with the shadowing spread. The interpretation is less intuitive, but we can think of shadowing as a low-frequency "noise" superimposed on the signal, whose power is directly proportional to its variability (as it occurs with thermal noise). Figures 8, 9 and 10 describe the behavior of the squared coefficient of variation. In particular, Figure 8 shows the dependence of this coefficient on distance, for different path-loss exponents. We can observe that the squared coefficient of variation decreases as the distance and/or the path-loss exponent increase, that is, as the expected energy harvested decreases. Such a reduction of variability with the decrease of the average is typical of non-negative random variables, like the energy harvested considered here. Figure 8 does not allow to distinguish between the curves obtained for the lowest path-loss exponents. However, these differences can be better highlighted by exchanging the roles of distance and path-loss exponent in the representation. This is shown in Figure 9, which confirms that beyond $\beta \cong 3.5$ the decay profiles begin to distinguish. Finally, Figure 10 shows how the squared coefficient of variation varies with the shadowing spread and the Nakagami parameter. As it can be noticed, the influence of the shadowing spread is much higher than that of the Nakagami parameter. The figure also highlights the fact that the squared coefficient of variation of the energy harvested can vary within a very large range, consistently with the relatively shorter variability of the shadowing spread.

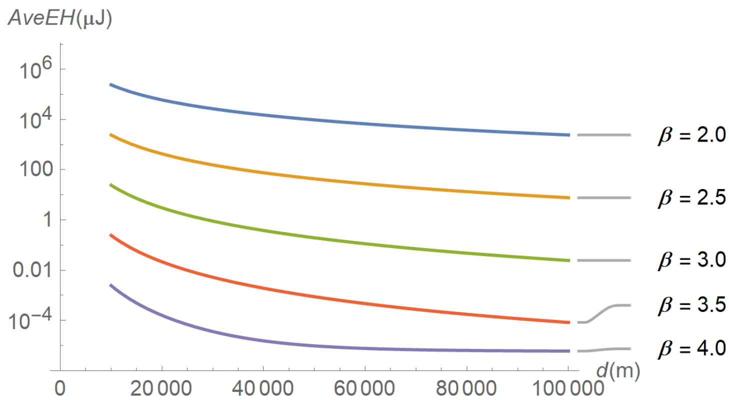

Figure 6. Evolution of the average energy harvested as a function of distance, for different path-loss exponents and a shadowing spread of 8.5 dB.

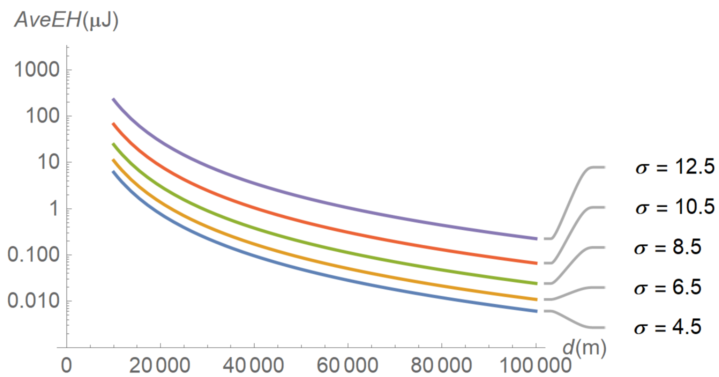

Figure 7. Evolution of the average energy harvested as a function of distance, for different levels of shadowing spread and a path-loss exponent equal to 3.0.

Preprints (www.preprints.org) | NOT PEER-REVIEWED | Posted: 6 September 2022 doi:10.20944/preprints202209.0083.v1

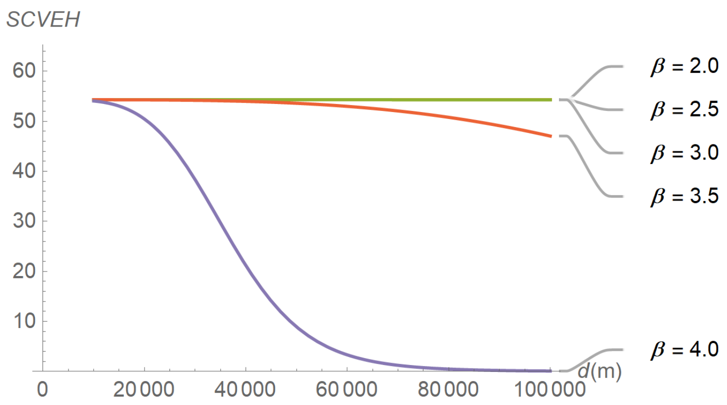

Figure 8. Evolution of the squared coefficient of variation in terms of distance, for different path-loss exponents. The shadowing spread and the Nakagami parameter have been set to 8.5 and 5.0, respectively.

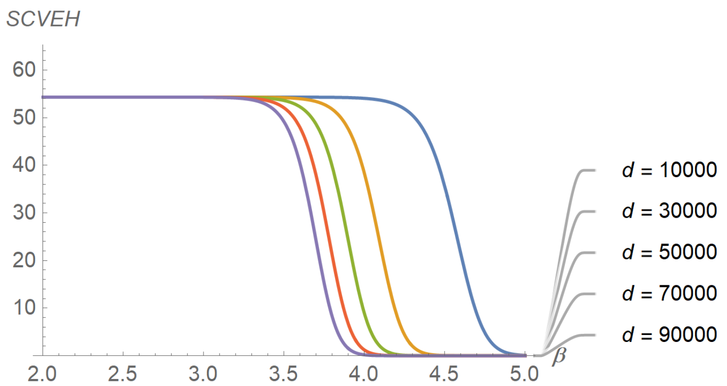

Figure 9. Evolution of the squared coefficient of variation in terms of the path-loss exponent, for different distances. The shadowing spread and the Nakagami parameter have been set to 8.5 and 5.0, respectively. The outermost curve corresponds to $d = 10000$ m.

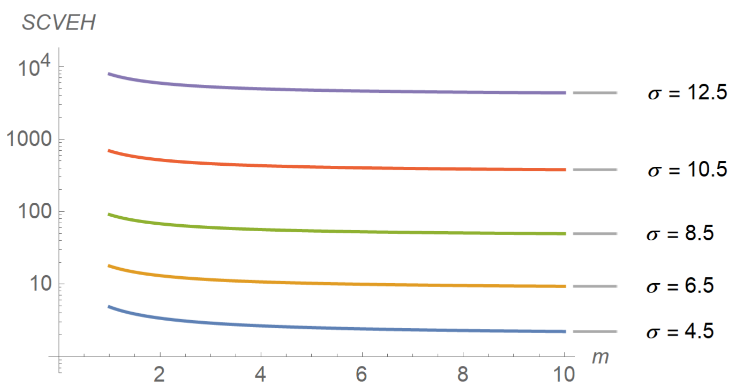

Figure 10. Evolution of the squared coefficient of variation as a function of the Nakagami parameter, for different values of the shadowing spread. The transmission distance and the path-loss exponent have been set to 50000 m. and 3.0, respectively.

7. Discussion

In this paper, exact closed-form expressions for the average and variance (and squared coefficient of variation) of the energy harvested by a static device have been obtained and validated via simulation. To model the propagation scenario, the Generalized-K model has been adopted, as it encompasses the effects of path-loss, shadowing and multi-path fading for a broad set of wireless scenarios. It has been assumed that the device is illuminated by a dedicated source that emits an unmodulated carrier during an arbitrary exposition time. A long-range scenario has also been assumed with the goal of highlighting the capabilities

 doi:10.20944/preprints202209.0083.v1

of the RF energy harvesting technology. The results obtained in this paper can be useful to design an energy transfer plan for scenarios with massive amounts of low-power devices, as expected with technologies like IoT and 5G and beyond. Particularly, the results obtained in this paper reveal that the path-loss and shadowing components of propagation have a much larger influence than multi-path fading in the energy harvesting process.

Future work may consist of applying the obtained formulation to analyze the effects of system parameters on the statistical behavior of the RF power harvested by energy-demanding devices. Also, the proposed formulation can be applied to several issues in the context of future wireless energy networks (network deployment, queuing performance). Finally, the work performed in this paper can be extended to mobile devices.

Funding: This research received no external funding.

Institutional Review Board Statement: Not applicable.

Informed Consent Statement: Not applicable.

Data Availability Statement: Not applicable.

Acknowledgments: The author would like to thank the anonymous reviewers of this journal for their helpful comments.

Conflicts of Interest: The author declares no conflict of interest.

Abbreviations

The following abbreviations are used in this manuscript:

5G/6G	Fifth/sixth generation
AWGN	Additive white Gaussian noise
CSI	Channel state information
EH	Energy harvesting
IoT	Internet of things
LOS	Line of sight
NLOS	Non line of sight
RF	Radio frequency
SWIPT	Simultaneous wireless information and power transfer
UAV	Unmanned autonomous vehicle
WIPT	Wireless information and power transfer
WIT	Wireless information transfer
WPT	Wireless power transfer

Appendix A

As stated in Section 5, the variance of the energy harvested is based on the expectation $E\{\|\tilde{r}(s)\|^2\|\tilde{r}(t)\|^2\}$. By recalling equation (16), the argument of such expectation can be formulated as follows:

$$\begin{aligned}\|\tilde{r}(s)\|^2\|\tilde{r}(t)\|^2 = &\Big(\|\tilde{x}(s)\|^2\|h(s)\|^2 + \tilde{n}_I^2(s) + \tilde{n}_Q^2(s) \\ &+ 2\Big(\tilde{x}_I(s)\cdot h_{re}(s) - \tilde{x}_Q(s)\cdot h_{im}(s)\Big)\cdot \tilde{n}_I(s) + 2\Big(\tilde{x}_I(s)\cdot h_{im}(s) + \tilde{x}_Q(s)\cdot h_{re}(s)\Big)\cdot \tilde{n}_Q(s)\Big) \\ &\cdot \Big(\|\tilde{x}(t)\|^2\|h(t)\|^2 + \tilde{n}_I^2(t) + \tilde{n}_Q^2(t) \\ &+ 2\Big(\tilde{x}_I(t)\cdot h_{re}(t) - \tilde{x}_Q(t)\cdot h_{im}(t)\Big)\cdot \tilde{n}_I(t) + 2\Big(\tilde{x}_I(t)\cdot h_{im}(t) + \tilde{x}_Q(t)\cdot h_{re}(t)\Big)\cdot \tilde{n}_Q(t)\Big)\end{aligned} \quad \text{(A.1)}$$

Preprints (www.preprints.org) | NOT PEER-REVIEWED | Posted: 6 September 2022 doi:10.20944/preprints202209.0083.v1

To evaluate the expected value of such a long expression, we can first identify the following terms:

- $I_1 : \|\tilde{x}(s)\|^2 \|h(s)\|^2$
- $I_2 : 2\Big(\tilde{x}_I(s) \cdot h_{re}(s) - \tilde{x}_Q(s) \cdot h_{im}(s)\Big) \cdot \tilde{n}_I(s) + 2\Big(\tilde{x}_I(s) \cdot h_{im}(s) + \tilde{x}_Q(s) \cdot h_{re}(s)\Big) \cdot \tilde{n}_Q(s)$
- $I_3 : \tilde{n}_I^2(s) + \tilde{n}_Q^2(s)$
- $I_4 : \|\tilde{x}(t)\|^2 \|h(t)\|^2$
- $I_5 : 2\Big(\tilde{x}_I(t) \cdot h_{re}(t) - \tilde{x}_Q(t) \cdot h_{im}(t)\Big) \cdot \tilde{n}_I(t) + 2\Big(\tilde{x}_I(t) \cdot h_{im}(t) + \tilde{x}_Q(t) \cdot h_{re}(t)\Big) \cdot \tilde{n}_Q(t)$
- $I_6 : \tilde{n}_I^2(t) + \tilde{n}_Q^2(t)$

Note that I_1, I_2 and I_3 are formally equivalent to I_4, I_5 and I_6, respectively. According to these new variables, equation (A.1) can be simply reformulated in the following way:

$$\|\tilde{r}(s)\|^2 \|\tilde{r}(t)\|^2 = (I_1 + I_2 + I_3) \cdot (I_4 + I_5 + I_6) \tag{A.2}$$

The subsequent procedure consists of developing all terms generated by the product in equation (A.2), and then take their respective expectations. In fact, only six out of the nine terms lead to different results:

Product $I_1 \cdot I_4$

$$I_1 \cdot I_4 = \|\tilde{x}(s)\|^2 \|h(s)\|^2 \|\tilde{x}(t)\|^2 \|h(t)\|^2 \tag{A.3}$$

Then, the expected value can be obtained after several manipulations:

$$\begin{aligned} E\{I_1 \cdot I_4\} &= E\Big\{\|\tilde{x}(s)\|^2 \|h(s)\|^2 \|\tilde{x}(t)\|^2 \|h(t)\|^2\Big\} \\ &= E\Big\{\|\tilde{x}(s)\|^2 \|\tilde{x}(t)\|^2\Big\} E\Big\{\|h(s)\|^2 \|h(t)\|^2\Big\} \\ &= E\Big\{\|\tilde{x}(t+\tau)\|^2 \|\tilde{x}(t)\|^2\Big\} E\Big\{\|h(t+\tau)\|^2 \|h(t)\|^2\Big\} \\ &= \phi_{\|\tilde{x}\|^2}(t,\tau) \cdot \phi_{\|h\|^2}(\tau) \end{aligned} \tag{A.4}$$

Note that the total expectation has been expressed as a product of expectations thanks to the independence between $\tilde{x}(t)$ and $h(t)$. Moreover, the temporal variable s has been replaced, with no loss of generality, by $t + \tau$, where τ is a time lag. The first expectation is nothing else but the auto-correlation of the squared module of $\tilde{x}$ in terms of the absolute time and the time lag τ, because no assumption has yet been made about the input signal being stationary (it depends on the type of modulation). Instead, since the channel is assumed to be stationary, the second auto-correlation depends exclusively on the time lag.

Product $I_1 \cdot I_5$

$$\begin{aligned} I_1 \cdot I_5 = 2\|\tilde{x}(s)\|^2 \|h(s)\|^2 \cdot \bigg(\Big(\tilde{x}_I(t) \cdot h_{re}(t) - \tilde{x}_Q(t) \cdot h_{im}(t)\Big) \cdot \tilde{n}_I(t) \\ + \Big(\tilde{x}_I(t) \cdot h_{im}(t) + \tilde{x}_Q(t) \cdot h_{re}(t)\Big) \cdot \tilde{n}_Q(t)\bigg) \end{aligned} \tag{A.5}$$

Since noise is independent of both input signal and channel coefficient, the expected value of the previous expression depends directly on the expected values of the in-phase and

 doi:10.20944/preprints202209.0083.v1

quadrature components of noise, which are identically zero: $E\{\tilde{n}_I(t)\} = E\{\tilde{n}_Q(t)\} = 0$. Accordingly:

$$E\{I_1 \cdot I_5\} = 0 \tag{A.6}$$

Product $I_1 \cdot I_6$

$$I_1 \cdot I_6 = \|\tilde{x}(s)\|^2 \|h(s)\|^2 \left(\tilde{n}_I^2(t) + \tilde{n}_Q^2(t)\right) \tag{A.7}$$

Again because of the mutual independence between input signal and channel coefficient, we have:

$$\begin{aligned} E\{I_1 \cdot I_6\} &= E\left\{\|\tilde{x}(s)\|^2\right\} E\left\{\|h(s)\|^2\right\} E\left\{\left(\tilde{n}_I^2(t) + \tilde{n}_Q^2(t)\right)\right\} \\ &= E\left\{\|\tilde{x}(s)\|^2\right\} E\left\{\|h(s)\|^2\right\} \left(E\left\{\tilde{n}_I^2(t)\right\} + E\left\{\tilde{n}_Q^2(t)\right\}\right) \\ &= 2N_R \cdot E\left\{\|\tilde{x}(s)\|^2\right\} E\left\{\|h(s)\|^2\right\} \end{aligned} \tag{A.8}$$

Here, the first property of AWGN stated in Section 4 has been recalled.

Product $I_2 \cdot I_4$

This product is formally equivalent to $I_1 \cdot I_5$; thus, we have:

$$E\{I_2 \cdot I_4\} = 0 \tag{A.9}$$

Product $I_2 \cdot I_5$

$$\begin{aligned} I_2 \cdot I_5 = 4\Big(&\left(\tilde{x}_I(s) \cdot h_{re}(s) - \tilde{x}_Q(s) \cdot h_{im}(s)\right) \cdot \tilde{n}_I(s) \\ &\cdot \left(\tilde{x}_I(t) \cdot h_{re}(t) - \tilde{x}_Q(t) \cdot h_{im}(t)\right) \cdot \tilde{n}_I(t) \\ &+ \left(\tilde{x}_I(s) \cdot h_{re}(s) - \tilde{x}_Q(s) \cdot h_{im}(s)\right) \cdot \tilde{n}_I(s) \\ &\cdot \left(\tilde{x}_I(t) \cdot h_{im}(t) + \tilde{x}_Q(t) \cdot h_{re}(t)\right) \cdot \tilde{n}_Q(t) \\ &+ \left(\tilde{x}_I(s) \cdot h_{im}(s) + \tilde{x}_Q(s) \cdot h_{re}(s)\right) \cdot \tilde{n}_Q(s) \\ &\cdot \left(\tilde{x}_I(t) \cdot h_{re}(t) - \tilde{x}_Q(t) \cdot h_{im}(t)\right) \cdot \tilde{n}_I(t) \\ &+ \left(\tilde{x}_I(s) \cdot h_{im}(s) + \tilde{x}_Q(s) \cdot h_{re}(s)\right) \cdot \tilde{n}_Q(s) \\ &\cdot \left(\tilde{x}_I(t) \cdot h_{im}(t) + \tilde{x}_Q(t) \cdot h_{re}(t)\right) \cdot \tilde{n}_Q(t)\Big) \end{aligned} \tag{A.10}$$

This expression involves the following expectations:

$$\begin{aligned} E\{\tilde{n}_I(s) \cdot \tilde{n}_I(t)\} &= E\{\tilde{n}_I(t+\tau) \cdot \tilde{n}_I(t)\} = \phi_I^{noise}(\tau) \\ E\{\tilde{n}_I(s) \cdot \tilde{n}_Q(t)\} &= E\{\tilde{n}_I(s)\} \cdot E\{\tilde{n}_Q(t)\} = 0 \cdot 0 = 0 \\ E\{\tilde{n}_Q(s) \cdot \tilde{n}_I(t)\} &= E\{\tilde{n}_Q(s)\} \cdot E\{\tilde{n}_I(t)\} = 0 \cdot 0 = 0 \\ E\{\tilde{n}_Q(s) \cdot \tilde{n}_Q(t)\} &= E\{\tilde{n}_Q(t+\tau) \cdot \tilde{n}_Q(t)\} = \phi_Q^{noise}(\tau) \end{aligned} \tag{A.11}$$

Note that the fact that noise is stationary and that its in-phase and quadrature components are independent (Section 4) has been taken into account. On the other hand, from [14] we

Preprints (www.preprints.org) | NOT PEER-REVIEWED | Posted: 6 September 2022 doi:10.20944/preprints202209.0083.v1

have $\phi_I^{noise}(\tau) = \phi_Q^{noise}(\tau) = \phi_{\tilde{n}}(\tau)$. Then, based on these preliminary results, the expected value of $I_2 \cdot I_5$ can be initially written as follows:

$$\begin{aligned} E\{I_2 \cdot I_5\} = 4E\Big\{ & \Big(\tilde{x}_I(s) \cdot h_{re}(s) - \tilde{x}_Q(s) \cdot h_{im}(s)\Big) \\ & \cdot \Big(\tilde{x}_I(t) \cdot h_{re}(t) - \tilde{x}_Q(t) \cdot h_{im}(t)\Big)\Big\} \cdot \phi_{\tilde{n}}(\tau) \\ & + 4E\Big\{\Big(\tilde{x}_I(s) \cdot h_{im}(s) + \tilde{x}_Q(s) \cdot h_{re}(s)\Big) \\ & \cdot \Big(\tilde{x}_I(t) \cdot h_{im}(t) + \tilde{x}_Q(t) \cdot h_{re}(t)\Big)\Big\} \cdot \phi_{\tilde{n}}(\tau) \end{aligned} \tag{A.12}$$

Next, by performing standard calculations, the latter equation can be rewritten in this way:

$$\begin{aligned} E\{I_2 \cdot I_5\} = {} & 4E\Big\{\Re\{\tilde{x}(s) \cdot h(s)\}\Re\{\tilde{x}(t) \cdot h(t)\}\Big\} \cdot \phi_{\tilde{n}}(\tau) \\ & + 4E\Big\{\Im\{\tilde{x}(s) \cdot h(s)\}\Im\{\tilde{x}(t) \cdot h(t)\}\Big\} \cdot \phi_{\tilde{n}}(\tau) \end{aligned} \tag{A.13}$$

Here, $\Im$ stands for the imaginary part. Given the linearity of the expectation operator, the latter result can be further simplified:

$$\begin{aligned} E\{I_2 \cdot I_5\} = {} & 4\phi_{\tilde{n}}(\tau) \\ & \cdot E\Big\{\Re\{\tilde{x}(s) \cdot h(s)\}\Re\{\tilde{x}(t) \cdot h(t)\} \\ & + \Im\{\tilde{x}(s) \cdot h(s)\}\Im\{\tilde{x}(t) \cdot h(t)\}\Big\} \\ & = 4\phi_{\tilde{n}}(\tau)E\Big\{\Re\Big\{\tilde{x}(s) \cdot h(s)\Big(\tilde{x}(t) \cdot h(t)\Big)^*\Big\}\Big\} \end{aligned} \tag{A.14}$$

Recall that the asterisk denotes the complex conjugate operator. Now, we can replace s by $t + \tau$ and formulate $E\{I_2 \cdot I_5\}$ in terms of correlations:

$$\begin{aligned} E\{I_2 \cdot I_5\} = {} & 4\phi_{\tilde{n}}(\tau) \\ & \cdot E\Big\{\Re\Big\{\tilde{x}(t+\tau) \cdot h(t+\tau)\Big(\tilde{x}(t) \cdot h(t)\Big)^*\Big\}\Big\} \\ & = 4\phi_{\tilde{n}}(\tau)\Re\Big\{E\{\tilde{x}(t+\tau) \cdot \tilde{x}^*(t) \cdot h(t+\tau) \cdot h(t)^*\}\Big\} \\ & = 4\phi_{\tilde{n}}(\tau)\Re\Big\{E\{\tilde{x}(t+\tau) \cdot \tilde{x}^*(t)\} \cdot E\{h(t+\tau) \cdot h(t)^*\}\Big\} \\ & = 4\phi_{\tilde{n}}(\tau)\Re\Big\{2\phi_{\tilde{x}}(t,\tau)2\phi_h(\tau)\Big\} \\ & = 16\phi_{\tilde{n}}(\tau)\Re\Big\{\phi_{\tilde{x}}(t,\tau)\phi_h(\tau)\Big\} \end{aligned} \tag{A.15}$$

Note from [15] that, in the complex field, $\phi_{U \cdot V} = \frac{1}{2}E\{U \cdot V^*\}$.

Product $I_2 \cdot I_6$

$$\begin{aligned} I_2 \cdot I_6 = 2\Big(\tilde{n}_I^2(t) + \tilde{n}_Q^2(t)\Big) & \\ \cdot \Big(\Big(\tilde{x}_I(s) \cdot h_{re}(s) - \tilde{x}_Q(s) \cdot h_{im}(s)\Big) \cdot \tilde{n}_I(s) & \\ + \Big(\tilde{x}_I(s) \cdot h_{im}(s) + \tilde{x}_Q(s) \cdot h_{re}(s)\Big) \cdot \tilde{n}_Q(s)\Big) & \end{aligned} \tag{A.16}$$

 doi:10.20944/preprints202209.0083.v1

Now, we can determine the corresponding expected value by making use of the independence properties already outlined:

$$\begin{aligned}E\{I_2\cdot I_6\} = 2E&\Big\{\Big(\tilde{x}_I(s)\cdot h_{re}(s)-\tilde{x}_Q(s)\cdot h_{im}(s)\Big)\Big\}\\ &\cdot E\Big\{\Big(\tilde{n}_I^2(t)+\tilde{n}_Q^2(t)\Big)\cdot\tilde{n}_I(s)\Big\}\\ &+2E\Big\{\Big(\tilde{x}_I(s)\cdot h_{im}(s)+\tilde{x}_Q(s)\cdot h_{re}(s)\Big)\Big\}\\ &\cdot E\Big\{\Big(\tilde{n}_I^2(t)+\tilde{n}_Q^2(t)\Big)\cdot\tilde{n}_Q(s)\Big\}\end{aligned} \tag{A.17}$$

Note that this formula relies on four expectations that only involve noise, namely $E\{\tilde{n}_I^2(t)\cdot\tilde{n}_I(s)\}$, $E\Big\{\tilde{n}_Q^2(t)\cdot\tilde{n}_I(s)\Big\}$, $E\{\tilde{n}_I^2(t)\cdot\tilde{n}_Q(s)\}$ and $E\Big\{\tilde{n}_Q^2(t)\cdot\tilde{n}_Q(s)\Big\}$. Two of them are zero as a result of the statistical independence between the in-phase and quadrature components of the equivalent low-pass noise signal:

$$E\Big\{\tilde{n}_Q^2(t)\cdot\tilde{n}_I(s)\Big\} = E\Big\{\tilde{n}_Q^2(t)\Big\}\cdot E\{\tilde{n}_I(s)\} = N_R\cdot 0 = 0 \tag{A.18}$$

$$E\Big\{\tilde{n}_I^2(t)\cdot\tilde{n}_Q(s)\Big\} = E\Big\{\tilde{n}_I^2(t)\Big\}\cdot E\{\tilde{n}_Q(s)\} = N_R\cdot 0 = 0 \tag{A.19}$$

On the other hand, since $\tilde{n}_I(t)$ is a zero-mean normal random process, any set of random variables obtained from it by selecting particular time instants constitute a zero-mean multivariate normal random vector. Hence, it satisfies the Isserlis' theorem [16], which states that any odd-order moment of a zero-mean multivariate normal random vector is zero. Accordingly:

$$E\Big\{\tilde{n}_I^2(t)\cdot\tilde{n}_I(s)\Big\} = 0 \tag{A.20}$$

The same statements can be formulated about process $\tilde{n}_Q(t)$ to conclude that:

$$E\Big\{\tilde{n}_Q^2(t)\cdot\tilde{n}_Q(s)\Big\} = 0 \tag{A.21}$$

Thus, we definitely have:

$$E\{I_2\cdot I_6\} = 0 \tag{A.22}$$

Product $I_3\cdot I_4$

As this product is formally equivalent to $I_1\cdot I_6$, we have:

$$E\{I_3\cdot I_4\} = E\{I_1\cdot I_6\} \tag{A.23}$$

Product $I_3\cdot I_5$

This product is formally equivalent to $I_2\cdot I_6$. Thus:

$$E\{I_3\cdot I_5\} = 0 \tag{A.24}$$

Product $I_3\cdot I_6$

$$I_3\cdot I_6 = \Big(\tilde{n}_I^2(s)+\tilde{n}_Q^2(s)\Big)\cdot\Big(\tilde{n}_I^2(t)+\tilde{n}_Q^2(t)\Big) \tag{A.25}$$

Preprints (www.preprints.org) | NOT PEER-REVIEWED | Posted: 6 September 2022 doi:10.20944/preprints202209.0083.v1

Its expectation is as follows:

$$\begin{aligned} E\{I_3 \cdot I_6\} &= E\Big\{\Big(\tilde{n}_I^2(s) + \tilde{n}_Q^2(s)\Big) \cdot \Big(\tilde{n}_I^2(t) + \tilde{n}_Q^2(t)\Big)\Big\} \\ &= E\Big\{\tilde{n}_I^2(s) \cdot \tilde{n}_I^2(t)\Big\} + E\Big\{\tilde{n}_I^2(s) \cdot \tilde{n}_Q^2(t)\Big\} \\ &+ E\Big\{\tilde{n}_Q^2(s) \cdot \tilde{n}_I^2(t)\Big\} + E\Big\{\tilde{n}_Q^2(s) \cdot \tilde{n}_Q^2(t)\Big\} \end{aligned} \tag{A.26}$$

This expression contains two types of expectations: those that involve both the in-phase and quadrature components of noise, and those that only involve one of these components. Regarding the latter, we can substitute s by $t + \tau$ and formulate them as auto-correlations, whereas for the former we can make use of the properties highlighted in Section 4:

$$\begin{aligned} E\{I_3 \cdot I_6\} &= E\Big\{\tilde{n}_I^2(t+\tau) \cdot \tilde{n}_I^2(t)\Big\} \\ &+ E\Big\{\tilde{n}_I^2(s)\Big\} \cdot E\Big\{\tilde{n}_Q^2(t)\Big\} \\ &+ E\Big\{\tilde{n}_Q^2(s)\Big\} \cdot E\Big\{\tilde{n}_I^2(t)\Big\} \\ &+ E\Big\{\tilde{n}_Q^2(t+\tau) \cdot \tilde{n}_Q^2(t)\Big\} \\ &= \phi_{\tilde{n}_I^2}(\tau) + N_R \cdot N_R + N_R \cdot N_R + \phi_{\tilde{n}_Q^2}(\tau) \\ &= 2N_R^2 + \phi_{\tilde{n}_I^2}(\tau) + \phi_{\tilde{n}_Q^2}(\tau) \end{aligned} \tag{A.27}$$

Next, by making use of the Isserlis' theorem for the even-order moments [16], we have:

$$\begin{aligned} \phi_{\tilde{n}_I^2}(\tau) &= E\Big\{\tilde{n}_I^2(t+\tau) \cdot \tilde{n}_I^2(t)\Big\} \\ &= E\{\tilde{n}_I(t+\tau) \cdot \tilde{n}_I(t+\tau) \cdot \tilde{n}_I(t) \cdot \tilde{n}_I(t)\} \\ &= E\{\tilde{n}_I(t+\tau) \cdot \tilde{n}_I(t+\tau)\} \cdot E\{\tilde{n}_I(t) \cdot \tilde{n}_I(t)\} \\ &+ E\{\tilde{n}_I(t+\tau) \cdot \tilde{n}_I(t)\} \cdot E\{\tilde{n}_I(t+\tau) \cdot \tilde{n}_I(t)\} \\ &+ E\{\tilde{n}_I(t+\tau) \cdot \tilde{n}_I(t)\} \cdot E\{\tilde{n}_I(t+\tau) \cdot \tilde{n}_I(t)\} \\ &= N_R \cdot N_R + 2\Big(\phi_I^{noise}(\tau)\Big)^2 = N_R^2 + 2\phi_{\tilde{n}}^2(\tau) \end{aligned} \tag{A.28}$$

Similarly:

$$\phi_{\tilde{n}_Q^2}(\tau) = N_R^2 + 2\phi_{\tilde{n}}^2(\tau) \tag{A.29}$$

Next, by introducing equations (A.28) and (A.29) into equation (A.27), and making some additional manipulations, we can obtain the following result:

$$E\{I_3 \cdot I_6\} = 4N_R^2 + 4\phi_{\tilde{n}}^2(\tau) \tag{A.30}$$

Finally, from equations (A.4), (A.6), (A.8), (A.9), (A.15), (A.22), (A.23), (A.24) and (A.30), we can derive the following expression for $E\{\|\tilde{r}(s)\|^2\|\tilde{r}(t)\|^2\}$, with $s = t + \tau$:

$$\begin{aligned} E\Big\{\|\tilde{r}(t+\tau)\|^2\|\tilde{r}(t)\|^2\Big\} &= \phi_{\|\tilde{x}\|^2}(t,\tau)\phi_{\|h\|^2}(\tau) \\ &+ 4N_R \cdot E\Big\{\|\tilde{x}(t)\|^2\Big\}E\Big\{\|h(t)\|^2\Big\} \\ &+ 16\phi_{\tilde{n}}(\tau) \cdot \Re\{\phi_{\tilde{x}}(t,\tau)\phi_h(\tau)\} \\ &+ 4N_R^2 + 4\phi_{\tilde{n}}^2(\tau) \end{aligned} \tag{A.31}$$

References

1. Lu, X; Wang, P; Niyato, D; Kim, D. I.; Han, Z. Wireless networks with RF energy harvesting: a contemporary survey. *IEEE Commun. Surveys & Tuts* **2015**, *17*, 757–789.
2. Tran, L; Cha, H; Park, W. RF power harvesting: a review on designing methodologies and applications. *Micro and Nano Syst Lett* **2017**, *5*.
3. Ponnimbaduge Perera, T. D.; Jayakody, D. N. K.; Sharma, S. K.; Chatzinotas, S.; Li, J. Simultaneous wireless information and power transfer (SWIPT): recent advances and future challenges. *IEEE Commun. Surveys & Tuts* **2018**, *20*, 264–302.
4. Jakayodi, D. N. K.; Thompson, J.; Chatzinotas, S.; Durrani, S. *Wireless Information and Power Transfer: A New Paradigm for Green Communications*; Springer: New York City, New York, USA, 2017.
5. Ng, D. W. K.; Duong, T. Q.; Zhong, C.; Schober, R. *Wireless Information and Power Transfer: Theory and Practice*; Wiley-IEEE Press: Hoboken, New Jersey, USA, 2018.
6. Hadzi-Velkov, Z.; Pejoski, S.; Schober, R.; Zlatanov, N. Wireless powered ALOHA networks with UAV-mounted-base stations. *IEEE Wireless Commun. Lett.* **2020**, *9*, 56–60.
7. Kumar, S.; De, S.; Mishra, D. RF energy transfer channel models for sustainable IoT. *IEEE Internet of Things Journal* **2018**, *5*, 2817–2828.
8. Luo, B,; Yeoh, P. L.; Schober, R.; Krongold, B. S. Optimal energy beamforming for distributed wireless power transfer over frequency-selective channels. In Proceedings of the IEEE International Conference on Communications, Shanghai, China, 20-24 May 2019.
9. Oliveira, D.; Oliveira, R. Characterization of energy availability in RF energy harvesting networks. *Mathematical Problems in Engineering* **2016**, 1–9.
10. Salahat, E.; Yang, N. Statistical models for battery recharge time from RF energy scavengers in generalized wireless fading channels. In Proceedings of IEEE Globecom Workshops, Singapore, Singapore, 4-8 December 2017.
11. Ju, H.; Zhang, R. Throughput maximization in wireless powered communication networks. *IEEE Trans. on Wireless Commun.* **2014**, *13*, 418–428.
12. Goldsmith, A. *Wireless Communications*; Cambridge University Press: Cambridge, UK, 2005.
13. Shankar, P. M. Outage probabilities in shadowed fading channels using a compound statistical model. *IEE Proceedings-Communications* **2005**, *152*, 828–832.
14. Proakis, J.; Manolakis, D. *Digital Signal Processing*, 4th ed.; Pearson: London, UK, 2013.
15. Papoulis, A.; Pillai, S. U. *Probability, Random Variables and Stochastic Processes*, 4th ed.; McGraw-Hill Europe: London, UK, 2002.
16. Isserlis, L. On a formula for the product-moment coefficient of any order of a normal frequency distribution in any number of variables. *Biometrika* **1918**, *12*, 134–139.
17. Stüber, G. L. *Principles of Mobile Communication*, 2nd ed; Kluwer Academic Publishers: Dordrecht, Netherlands, 2001.
18. Lladó, J.; Galmés, S. Wireless energy networks - how cooperation extends to energy. *Lecture Notes in Computer Science* **2022**, *13492*.

Short Biography of Authors

Sebastià Galmés (M'10) received the M.Sc. degree in Electrical Engineering from Polytechnic University of Catalonia, Barcelona, Spain, in 1989, and the Ph.D. degree in Computer Science from University of the Balearic Islands, Palma de Mallorca, Spain, in 1999, where he is currently Associate Professor in the Department of Mathematics and Computer Science. He is also member of the Health Research Institute of the Balearic Islands (Institut d'Investigació Sanitària de les Illes Balears - IdISBa). His current research interests focus on wireless communication protocol development, wireless sensor networks, nanoscale and molecular communications, with special emphasis on health applications, and RF energy harvesting.